Elementary processes in ternary solar cells

Teodoro Pizza[a,b], Alessandro Landi[a]*,
Francesco Ambrosio[c], Amedeo Capobianco[a]† and Andrea Peluso[a]

[a] *Dipartimento di Chimica e Biologia, Università di Salerno, Via Giovanni Paolo II, 132, I-84084 Fisciano (SA), Italy.*
[b] *Dipartimento di Chimica, Biologia e Biotecnologie, Università degli Studi di Perugia, Via Elce di Sotto, 8, I-06123 Perugia (PG), Italy.* [c] *Dipartimento di Scienze, Università degli Studi della Basilicata, Viale dell'Ateneo Lucano, 10 I-85100 Potenza (PZ), Italy.*

Electronic Supplementary Information

*To whom correspondence should be addressed. Email: alelandi1@unisa.it
†To whom correspondence should be addressed. Email: acapobianco@unisa.it

Contents

List of Figures

List of Tables

S1 Methods

S1.1 MD simulations

The donor/acceptor and donor/donor interfaces for the ternary FG3:FG4:Y6 cell have been characterized by performing classical molecular dynamics (MD) simulations on a cubic box containing 15 FG3 molecules, 35 FG4 molecules, and 75 Y6 molecules, thus reproducing the experimental relative abundance (0.12:0.28:0.60) of components.[1] The molecules have been randomly arranged to mimic a BHJ interface. After a 1 ns equilibration and 100 ns of simulated annealing, trajectories have been simulated for 100 ns.

For electronic coupling calculations, we sampled $\approx$ 100 molecular pairs (either D/D, or D/A, depending on the process under study) geometries from the last 40 ns of the simulation, at 500 ps intervals, to extract uncorrelated snapshots. We selected only molecules such that at least two atoms belonging to the interacting units is less than 5 Å and such that the long molecular axis was at least 90% of the length of the same axis at the equilibrium geometry.[2] The same protocol has been applied to the A/D interface for the binary blends FG3:Y6 and FG4:Y6. In both cases, the box is composed of 50 molecules of donor and 75 molecules of acceptor, i.e. the adopted composition match the experimental ratio (0.4:0.6).[1] Figure S1 shows the configurations yielding the fastest PET for FG3/Y6, FG4/Y6 and the most efficient FRET at FG3/FG4 interface in the ternary cell. We remark that this protocol has been followed on the basis of previous studies,[2,3] showing that it leads to a good description of the average behaviour of the cell, see also section S5 below.

S1.2 Electronic couplings

For PHT, PET and CR processes, the electronic couplings have been calculated as $J_{ij} = \langle \phi_i | \hat{F} | \phi_j \rangle$, where ϕ_i and ϕ_j are the unperturbed frontier Kohn-Sham orbitals of the isolated D and A, respectively, and $\hat{F}$ is the Kohn-Sham-Fock operator of the D/A pair.[4–6] Computations were carried out at the density functional level of theory (DFT) by using the CAM-B3LYP functional and the 3-21G* basis set.[7]

Electronic couplings for FRET and EET have been evaluated by means of a perturbative approach from the transition densities of the non-interacting units,[8] as implemented in the Gaussian package,[9] by using time dependent (TD) DFT, at the (TD)CAM-B3LYP/3-21G* level of theory. The highest electronic couplings are reported in Tables S1 and S2, whereas average couplings are given in Tables 1 and 2 of the main article. While in MD simulations all the alkyl substituents have been retained, they have been replaced by methyl groups in DFT and TD-DFT computations of electronic couplings.[2]

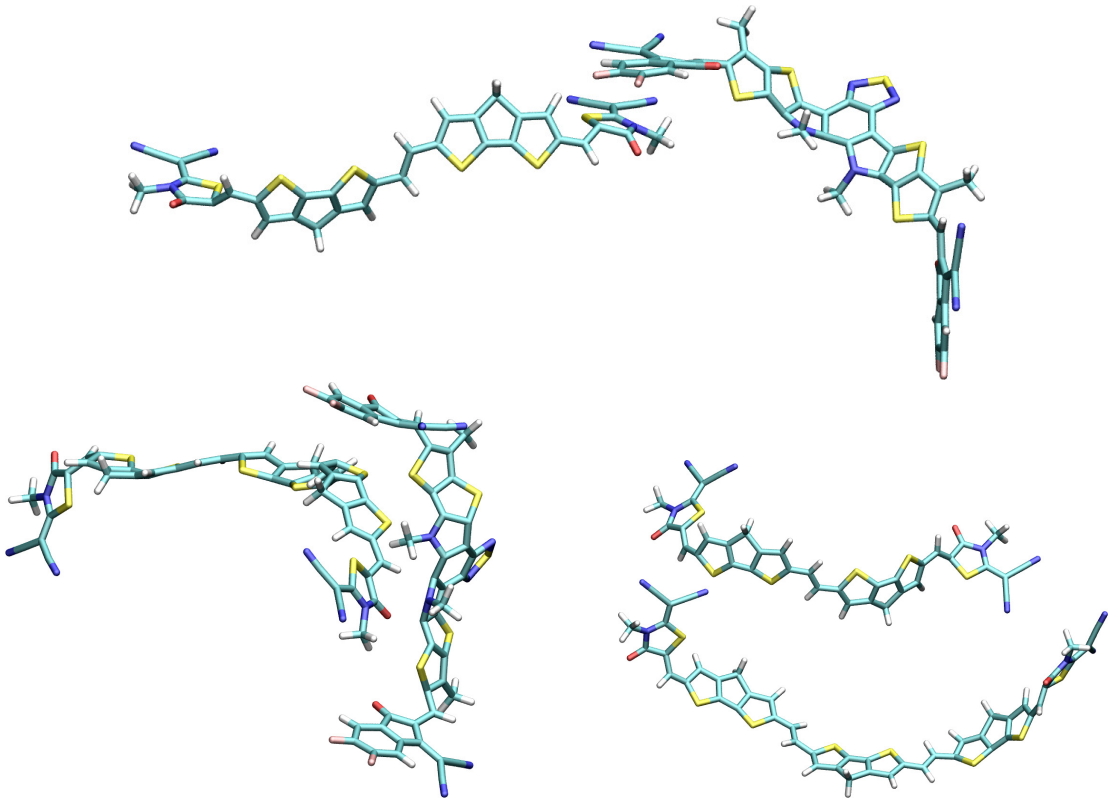

Fig. S1: Predicted (MD) configurations giving rise, in the ternary cell, to the highest PET coupling at the FG3/Y6 interface (top), FG4/Y6 interface (bottom left) and the highest FRET coupling FG3/FG4 interface (bottom right).

Table S1: Highest electronic couplings (meV) for the formation of charge transfer states (PET/PHT) at the D/A interfaces, for the charge recombination (CR) from the charge transfer states to the ground states and for the energy transfer (EET) in the binary devices.

Cell	PHT	PET	CR	EET
FG3:Y6	41.9	53.6	78.2	40.3
FG4:Y6	26.9	60.6	42.1	33.6

Table S2: Highest electronic couplings (meV) for the formation of charge transfer states (PET and PHT) and charge recombination (CR) at the D/A interfaces. Highest couplings for energy transfer (FRET) at the FG3/FG4 interface is also included. The corresponding configurations of binary complexes are depicted in Figure S1. All data refer to the ternary cell.

Interface	PHT	PET	CR	FRET
FG3/Y6	25.8	18.5	81.6	-
FG4/Y6	30.4	59.6	49.1	-
FG3/FG4	-	-	-	53.7

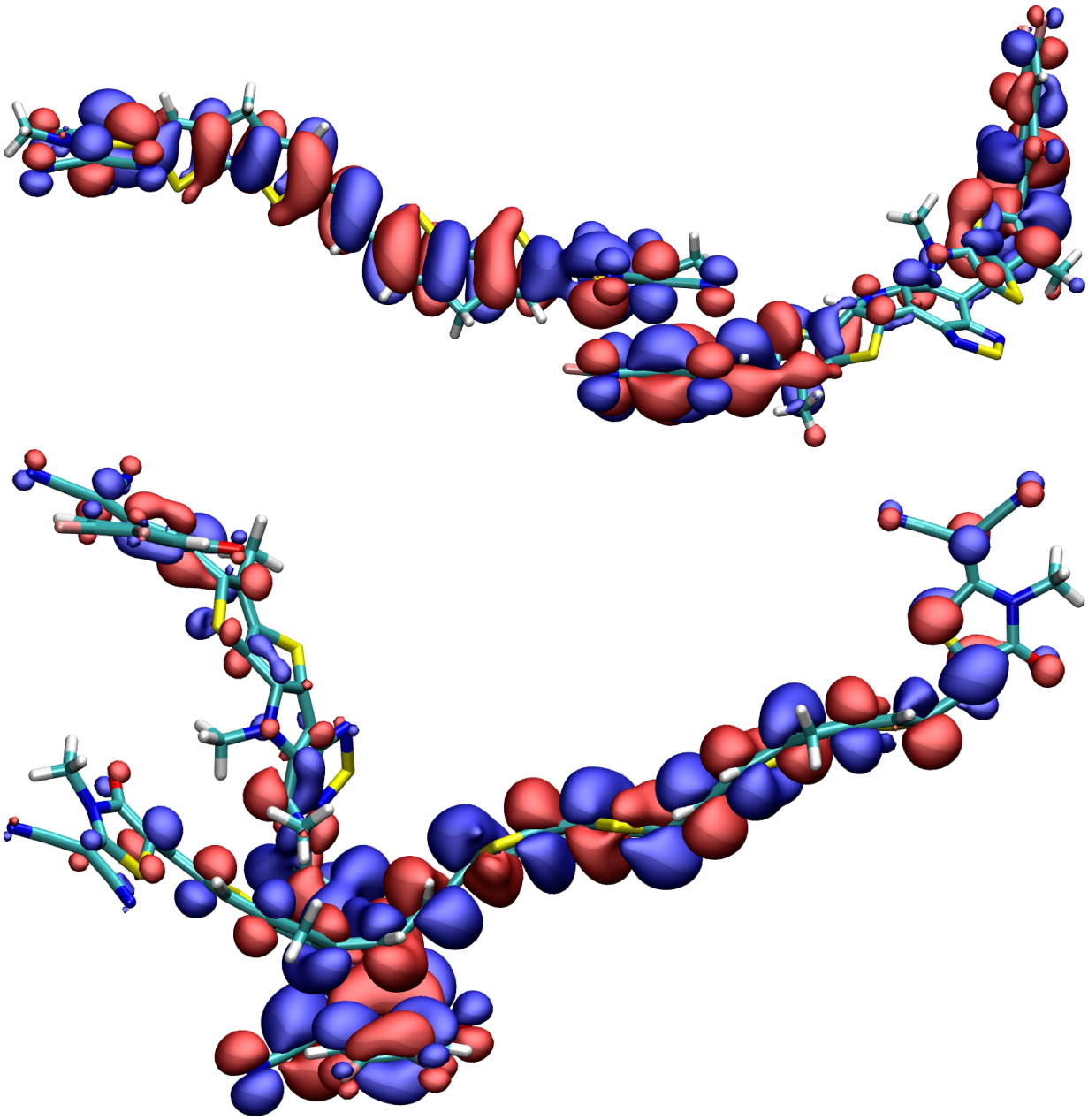

Fig. S2: Orbitals in CR for FG3:Y6 (top) and FG4:Y6 (bottom) in the ternary cell.

S1.3 Prediction of kinetic rates and lineshapes

To simplify the mathematical notation, at variance with the main text we will use uppercase letters (e.g. A) to identify electronic states, while lowercase letter to identify vibrational states of the corresponding electronic states (e.g. a is a vibrational state of the electronic state A).
Kinetic rates and spectral lineshapes have been computed by resorting to the so-called generating-function (GF) theory.[10] Details on the derivation and implementation of the GF formalism can be found elsewhere;[11] here we only summarize the main results.
According to Fermi's golden rule, the rate for an electronic transition from initial state A to final state B, can be expressed as:

$$k = \frac{2\pi}{\hbar}|J_{AB}|^2 F(\Delta E + \epsilon, T), \tag{S1}$$

where J_{AB} is the electronic coupling for A and B, F is the density of states, $\Delta E = E_B - E_A$,

$$\epsilon = \begin{cases} \pm\, h\nu & \text{radiative transition,} \\ -\Delta E & \text{non-radiative transition} \end{cases} \tag{S2}$$

and the plus (minus) sign in Eq. S2 refers to emission (absorption).
Upon introducing the Born-Oppenheimer approximation, we have for $X = A, B$:

$$|\mathrm{X}\rangle = |X, x\rangle = |X\rangle \otimes |x\rangle\,, \tag{S3}$$

$$\mathcal{E}_\mathrm{X} = E_X + \eta_x \tag{S4}$$

where $|X\rangle$ denotes a pure electronic state whose energy is E_X and $|x\rangle$ represents the vibronic states of X with energy η_x. Under the assumption that J_{AB} is independent of the nuclear coordinates (Condon approximation), the density of states (Eq. S1) can be cast in the form:[12]

$$F(\Delta E + \epsilon, T) = \sum_{a,b} |\,\langle b|a\rangle\,|^2 \mathrm{e}^{-\beta\eta_a}\delta(\mathcal{E}_B - \mathcal{E}_A + \epsilon)/Z_A, \tag{S5}$$

where T is temperature, $\beta = 1/(k_\mathrm{B}T)$, with k_B the Boltzmann constant, Z_A is the vibrational partition function of state A, and $\langle b|a\rangle$ are Franck-Condon integrals, so that F is the Franck-Condon weighted density of states (FCWD). By using the integral representation of the delta function, the FCWD can be written as:

$$F = \frac{1}{2\pi}\int_{-\infty}^{+\infty} \mathrm{e}^{\mathrm{i}(\Delta E+\epsilon)\tau} f(\tau)\,\mathrm{d}\tau \tag{S6}$$

where $\Delta E = E_B - E_A$ considers "purely electronic" energies (Eq. S4) and:

$$f(\tau) = \frac{\mathsf{Tr}\left[\mathrm{e}^{\mathrm{i}\tau\mathcal{H}_\mathrm{B}}\mathrm{e}^{-(\beta+\mathrm{i}\tau)\mathcal{H}_\mathrm{A}}\right]}{\mathsf{Tr}\left[\mathrm{e}^{-\beta\mathcal{H}_\mathrm{A}}\right]}, \tag{S7}$$

with $\mathcal{H}_\mathrm{A}(\mathcal{H}_\mathrm{B})$ being the vibrational Hamiltonian operator of the initial(final) electronic state. By assuming the harmonic model for vibrations and using mass-weighted vibrational coordinates, Kubo and Toyozawa were able to to put the correlation function into closed form.[10] Upon introducing normal coordinates and using the affine transformation proposed by Duschinsky to express one set of normal coordinates with respect to the other:[11,13]

$$\mathbf{Q}_B = \mathbf{J}\mathbf{Q}_A + \mathbf{K},$$

where $\mathbf{Q}$ denote normal coordinates, the Jacobian $\mathbf{J}$ is the Duschinsky matrix and $\mathbf{K}$ is the displacement vector, $f(\tau)$ assumes the form:

$$f(\tau) = [\det \mathbf{\Phi}]^{-1/2} \exp\left[-\mathbf{D}^\mathsf{T}\mathbf{T}_\mathrm{A}\left(\mathbf{T}_\mathrm{A}+\mathbf{T}_\mathrm{B}\right)^{-1}\mathbf{T}_\mathrm{B}\mathbf{D}\right], \tag{S8}$$

where:

$$\begin{aligned}
&\mathbf{T}_\mathrm{A} = \boldsymbol{\omega}_\mathrm{A}\tanh\left[(\beta-\mathrm{i}\tau)\boldsymbol{\omega}_\mathrm{A}/2\right]; \quad \mathbf{T}_\mathrm{B} = \mathbf{J}^\mathsf{T}\boldsymbol{\omega}_\mathrm{B}\tanh\left(\mathrm{i}\tau\boldsymbol{\omega}_\mathrm{B}/2\right)\mathbf{J}\\
&\mathbf{C}_\mathrm{A} = \boldsymbol{\omega}_\mathrm{A}/\tanh\left[(\beta-\mathrm{i}\tau)\boldsymbol{\omega}_\mathrm{A}/2\right]; \quad \mathbf{C}_\mathrm{B} = \mathbf{J}^\mathsf{T}\boldsymbol{\omega}_\mathrm{B}/\tanh\left(\mathrm{i}\tau\boldsymbol{\omega}_\mathrm{B}/2\right)\mathbf{J}\\
&\mathbf{\Phi} = \left[2\sinh\left(\beta\boldsymbol{\omega}_\mathrm{A}/2\right)\right]^{-2}{\boldsymbol{\omega}_\mathrm{A}}^{-1}\sinh\left[(\beta-\mathrm{i}\tau)\boldsymbol{\omega}_\mathrm{A}\right]\left(\mathbf{T}_\mathrm{A}+\mathbf{T}_\mathrm{B}\right)\left(\mathbf{C}_\mathrm{A}+\mathbf{C}_\mathrm{B}\right){\boldsymbol{\omega}_\mathrm{B}}^{-1}\sinh\left(\mathrm{i}\tau\boldsymbol{\omega}_\mathrm{B}\right)\\
&\mathbf{D} = \mathbf{J}^{-1}\mathbf{K}.
\end{aligned} \tag{S9}$$

Herein, T superscript denotes transpose, energies are expressed as wavenumbers, $\boldsymbol{\omega}_{\mathrm{A(B)}}$ is the diagonal matrix holding the harmonic vibrational wavenumbers for state A(B). The fraction bar symbol appearing in the expressions for $\mathbf{C}_\mathrm{A}$ and $\mathbf{C}_\mathrm{B}$ and connecting diagonal matrices, denotes division between corresponding diagonal elements.

For bimolecular processes (such as charge or energy transfer) involving two weakly interacting molecules, the final FCWD, $F(\Delta E, T)$ can be obtained by the convolution of the FCWD of the two half-reactions. For example, in the case of photo-electron transfer:

$$\begin{aligned}
&\mathrm{D}^* \rightarrow \mathrm{D}^+ + \mathrm{e}^-,\\
&\mathrm{A} + \mathrm{e}^- \rightarrow \mathrm{A}^-,
\end{aligned} \tag{S10}$$

where D^* is the donor molecule in its excited state and A is the acceptor molecule in its ground

state. The convolution is obtained as

$$F(\Delta E) = \int_{-\infty}^{\infty} \mathrm{d}E\, F_{\mathrm{D}}(E) F_{\mathrm{A}}(E - \Delta E), \tag{S11}$$

where F_{D} and F_{A} are the FCWD for the processes in Eq. S10.
Rates were determined by using Eq. S1 with the average couplings of Tables 1 and 2 of the main text and $F(\Delta E_{\mathrm{r}}, T = 298\ \mathrm{K})$, where ΔE_{r} is the reaction energy of the relevant process, namely:

$$\begin{aligned}
\Delta E_{\mathrm{PET,FG3}} &= \mathrm{IP(FG3)} - \mathrm{EA(Y6)} - E_{0-0}\mathrm{(FG3)},\\
\Delta E_{\mathrm{PET,FG4}} &= \mathrm{IP(FG4)} - \mathrm{EA(Y6)} - E_{0-0}\mathrm{(FG4)},\\
\Delta E_{\mathrm{PHT,FG3}} &= \mathrm{IP(FG3)} - \mathrm{EA(Y6)} - E_{0-0}\mathrm{(Y6)},\\
\Delta E_{\mathrm{PHT,FG4}} &= \mathrm{IP(FG4)} - \mathrm{EA(Y6)} - E_{0-0}\mathrm{(Y6)},\\
\Delta E_{\mathrm{CR,FG3}} &= \mathrm{EA(Y6)} - \mathrm{IP(FG3)},\\
\Delta E_{\mathrm{CR,FG4}} &= \mathrm{EA(Y6)} - \mathrm{IP(FG4)},\\
\Delta E_{\mathrm{EET,FG3}} &= E_{0-0}^{\mathrm{Y6}} - E_{0-0}^{\mathrm{FG3}},\\
\Delta E_{\mathrm{EET,FG4}} &= E_{0-0}^{\mathrm{Y6}} - E_{0-0}^{\mathrm{FG4}},\\
\Delta E_{\mathrm{FRET}} &= E_{0-0}^{\mathrm{FG4}} - E_{0-0}^{\mathrm{FG3}}.
\end{aligned} \tag{S12}$$

Adiabatic ionization energies (IP) and electron affinities (EA) used in previous equations are given in Table S3. They were set equal to the oxidation (reduction) free energies referred to vacuum. Oxidation and reduction free energies were obtained by Guijarro *et al.* (ref.s 1 and 14) by Osteryoung square wave voltammetry measurements carried out in orthodichlorobenzene:acetonitrile (4:1) solutions using ferrocenium/ferrocene (Fc^+/Fc) as the internal reference. The absolute reduction potential for the Fc^+/Fc couple has been set to 5.1 V, as in ref.s 1 and 14, but it elides in the differences (Eqn.s S12). E_{0-0} energies were estimated by aligning the predicted and observed FCWD for the $S_1 \leftarrow S_0$ absorption of FG3, FG4 and Y6. Indeed, as is well known, the FCWD for a radiative transition is related to emission intensity and molar absorption coefficient as:[15,16]

$$\begin{aligned}
I_{\mathrm{em}}(\nu) &\propto \nu^4 F(\Delta E + h\nu),\\
\eta(\nu) &\propto \nu F(\Delta E - h\nu).
\end{aligned} \tag{S13}$$

Because we set $\Delta\mathcal{E} = 0$ (Eq. S6) in the computations of FCWD's and because the FCWD must be normalized in the sense of unit area, upon aligning the FCWD extracted from the observed spectrum with the predicted one in such a way to maximize the overlap between the curves, it is possible to localize the position of the 0-0 transition energy. An example is given in Figure S3 for

Table S3: Ionization potentials (IP), electron affinities (EA) and 0-0 transition energies E_{0-0} used in computations. All data are expressed in eV.

	FG3	FG4	Y6
IP[a]	5.39	5.17	-
EA[a]	-	-	4.06
E^{b}_{0-0}	1.53	1.27	1.46

[a]For all the molecules, IP(EA) has been approximated as the oxidation(reduction) free energy referred to vacuum. Oxidation and reduction free energies were inferred by Osteryoung square wave voltammetry measurements carried out in orthodichlorobenzene:acetonitrile (4:1) solutions using ferrocenium/ferrocene (Fc^{+}/Fc) as the internal reference. The absolute reduction potential for the Fc^{+}/Fc couple has been set to 5.1 V, as in refs 14 and 1. [b]Obtained by aligning the predicted and observed FCWD for the $S_1 \leftarrow S_0$ absorption, see Figure S3.

the absorption of FG3. Comparison of observed and predicted FCWD shows a very good agreement between the computed and the experimental bandwidth for the lowest energy absorption. In the region of high wavenumbers the experimental FCWD exhibits a band peaked at ≈ 25000 cm^{-1} causing a slight enlargement of the experimental signal. That, however, corresponds to a transition to a higher excited electronic state of FG3, not considered in computations.

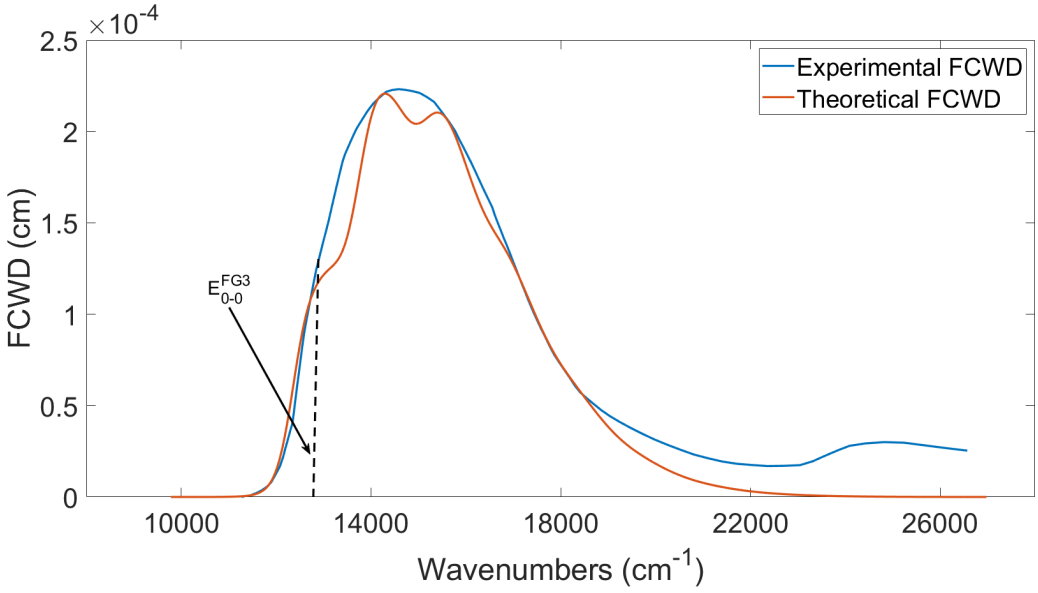

Fig. S3: Superimposition of the experimental(blue) and theoretical(orange) FCWDs for the $S_1 \leftarrow S_0$ absorption of FG3; the 0-0 transition energy is indicated by the black dashed vertical bar. The experimental absorption spectrum has been digitized from ref. [1]

The FCWD's for all the investigated processes and their relative ΔE_r are illustrated in Section

S4.

S2 Computational Details

Equilibrium geometries, vibrational frequencies and normal modes of vibration have been computed at the density functional theory (DFT) level, employing the CAM-B3LYP functional and the 6-31G* basis set via the Gaussian 16 package.[9] We settled on this particular functional and basis set because it has been already shown their ability to precisely describe long-range properties of extended π-conjugated systems, similar to the molecules considered here.[7,17] Time-dependent DFT (TD-DFT) was used to treat excited states. The polarizable continuum model (PCM) was used to take into account bulk polarization; the dielectric constant, ε, was set to 4, which is a suitable value for mimicking the environment in organic solid state devices.[2,18,19] The unrestricted formalism was adopted for species with unpaired electrons. Alkyl substituents have been replaced by methyl groups in DFT and TDDFT geometry optimizations and computations of the Hessian matrix.

MD simulations were carried out by using the GROMACS 2020.5 software.[20] The OPLS force field was adopted throughout.[21] Periodic boundary conditions were introduced and long range electrostatic effects were taken into account through the PME algorithm.[22] An integration time step of 2 fs was set up, by imposing constraints on the bonds involving H atoms through the LINCS algorithm,[23] adopting a modified Berendsen thermostat to control temperature and a Parrinello-Rahman barostat to control pressure.[24,25] The computational protocol consisted of an initial steepest descent minimisation, followed by a NVT equilibration in at 300 K over 1 ns. The system was then subjected to 5 simulated annealing (SA) cycles over 100 ns, between 300 K and 600 K, adopting the NPT ensemble: heatings and coolings were run over 500 ps intervals, the target temperature was maintained for 9.5 ns. Finally, a production run of 100 ns in the NPT ensemble was carried out.

S3 Kinetic model for binary cells

We have set up a kinetic model for state populations,[2,26] described by the following set of coupled differential equations:

$$\frac{\mathrm{d}}{\mathrm{d}t}\begin{pmatrix} P_{\mathrm{GS}} \\ P_{\mathrm{D}^*} \\ P_{\mathrm{A}^*} \\ P_{\mathrm{CT}} \end{pmatrix} = \begin{pmatrix} 0 & 0 & 0 & k_{\mathrm{CR}} \\ 0 & -(k_{\mathrm{EET}} + k_{\mathrm{PET}}) & 0 & 0 \\ 0 & k_{\mathrm{EET}} & -k_{\mathrm{PHT}} & 0 \\ 0 & k_{\mathrm{PET}} & k_{\mathrm{PHT}} & -k_{\mathrm{CR}} \end{pmatrix} \begin{pmatrix} P_{\mathrm{GS}} \\ P_{\mathrm{D}^*} \\ P_{\mathrm{A}^*} \\ P_{\mathrm{CT}} \end{pmatrix} \tag{S14}$$

where P is the (normalized) population and the labels GS, D^*, A^*, CT refer, respectively, to the ground state, the locally excited donor, the locally excited acceptor, and the charge transfer state. The matrix of rate constants has been built according to the model of electronic states and processes reported in the main text, Fig 1.

S4 Predicted FCWD and energy for charge transfer and energy transfer reactions

FCWDs computations have been carried out through the MolFC software package.[27] Rate constants have been computed evaluating $F(\Delta E_r, T)$ at $T = 298$ K and the proper ΔE_r, by averaging the FCWD over a small interval around that energy (200 cm^{-1}), a practical way to account for thermal disorder. Convoluted FCWD's as well as adopted ΔE_r are shown in Figures S4-S12.

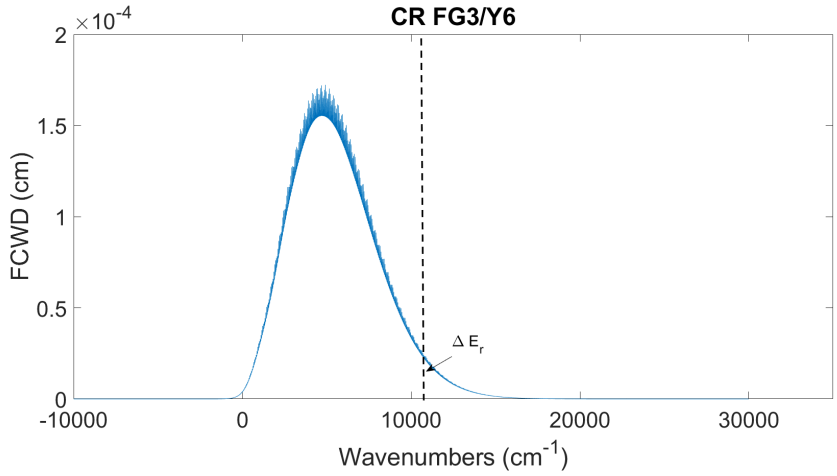

Fig. S4: FCWD for the charge recombination of $FG3^+$ with $Y6^-$ obtained by convolution of the FCWDs for the $FG3^+ \rightarrow FG3$ and $Y6^- \rightarrow Y6$ processes. The black dashed line indicates the energy of the reaction (ΔE_r) at which the FCWD is evaluated.

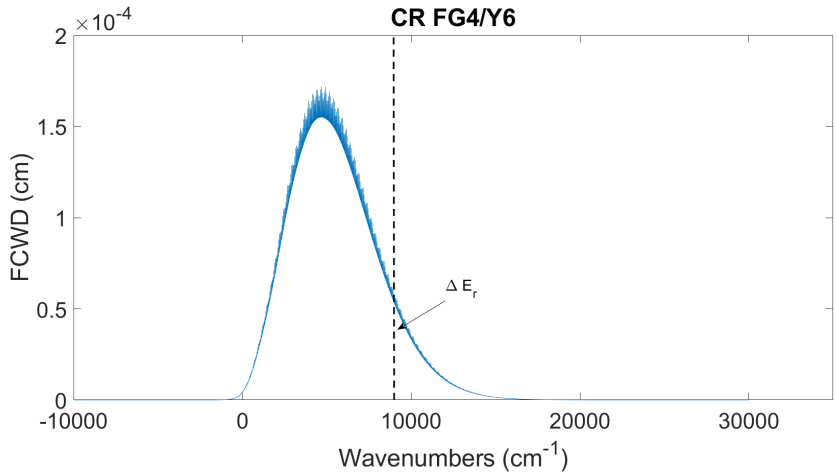

Fig. S5: FCWD for the charge recombination of $FG4^+$ with $Y6^-$ obtained by convolution of the FCWDs for the $FG4^+$ →FG4 and $Y6^-$ →Y6 processes. The black dashed line represents the energy of the reaction (ΔE_r) at which the FCWD is evaluated.

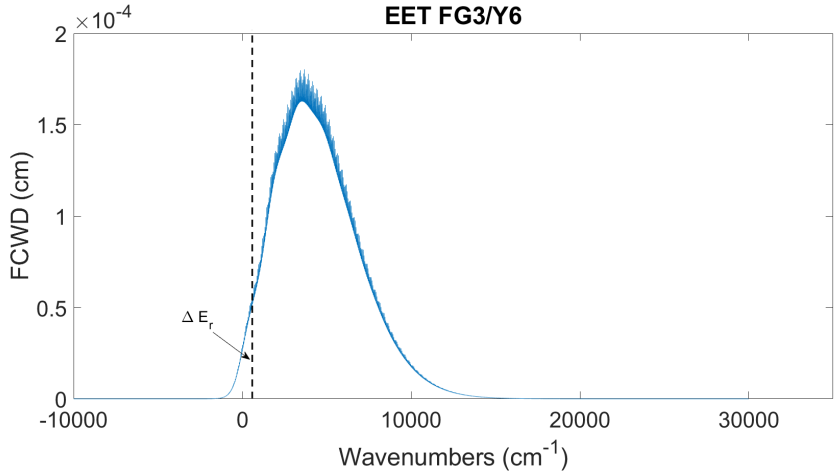

Fig. S6: FCWD for the excitation energy transfer process Y6+$FG3^*$→$Y6^*$+FG3 obtained by convolution of the FCWDs for the $FG3^*$ →FG3 and Y6→$Y6^*$ processes. The black dashed line indicates the energy of the reaction (ΔE_r) at which the FCWD is evaluated.

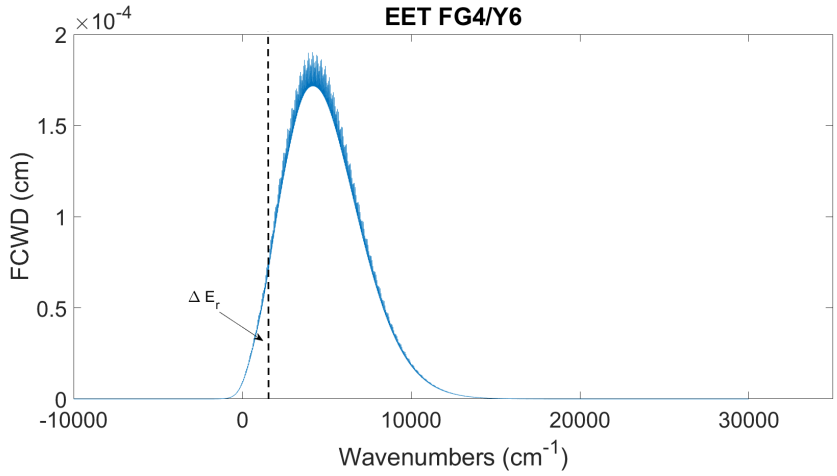

Fig. S7: FCWD for the excitation energy transfer process Y6 + FG4* → Y6* + FG4. Since EET for FG4 to Y6 is an endoergic process, the rate for the inverse reaction has been firstly evaluated through the convolution of the FCWDs for the FG4 → FG4* and Y6* → Y6 processes. The black dashed line indicates the energy of the inverse reaction (ΔE_{r}). The direct rate has been determined by means of the principle of detailed balance.[28,29]

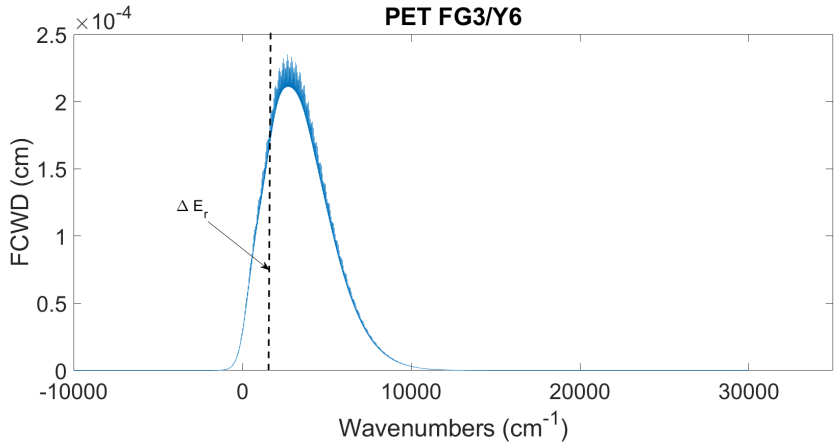

Fig. S8: FCWD for the photoelectron transfer process Y6+FG3*→Y6$^-$+FG3$^+$obtained by convolution of the FCWDs for the FG3* →FG3$^+$ and Y6→Y6$^-$ processes. The black dashed line indicates the energy of the reaction (ΔE_{r}) at which the FCWD is evaluated.

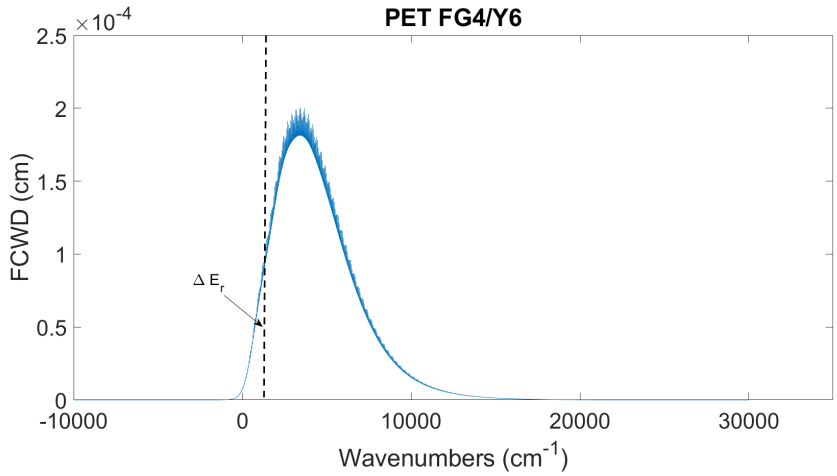

Fig. S9: FCWD for the photoelectron transfer process $\mathrm{Y6} + \mathrm{FG4}^* \rightarrow \mathrm{Y6}^- + \mathrm{FG4}^+$ obtained by convolution of the FCWDs for the $\mathrm{FG4}^* \rightarrow \mathrm{FG4}^+$ and $\mathrm{Y6} \rightarrow \mathrm{Y6}^-$ processes. The black dashed line indicates the energy of the reaction (ΔE_r) at which the FCWD is evaluated.

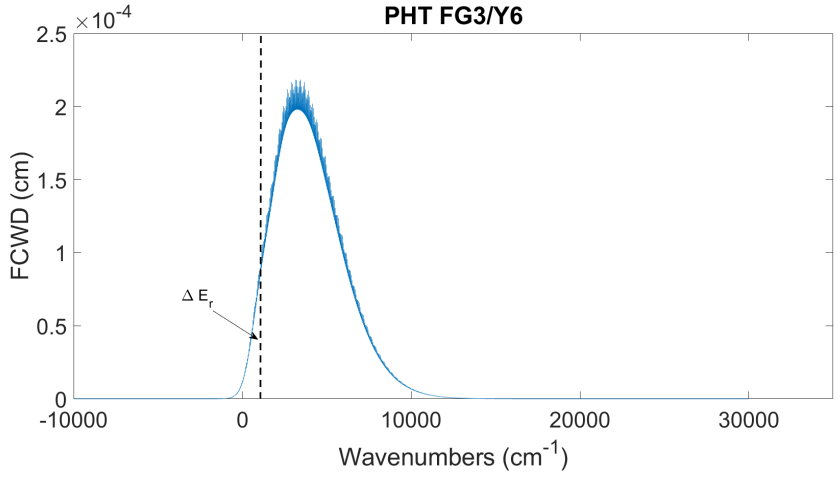

Fig. S10: FCWD for the photohole transfer process $\mathrm{Y6}^* + \mathrm{FG3} \rightarrow \mathrm{Y6}^- + \mathrm{FG3}^+$ obtained by convolution of the FCWDs for the $\mathrm{Y6}^* \rightarrow \mathrm{Y6}^-$ and $\mathrm{FG3} \rightarrow \mathrm{FG3}^+$ processes. The black dashed line indicates the energy of the reaction (ΔE_r) at which the FCWD is evaluated.

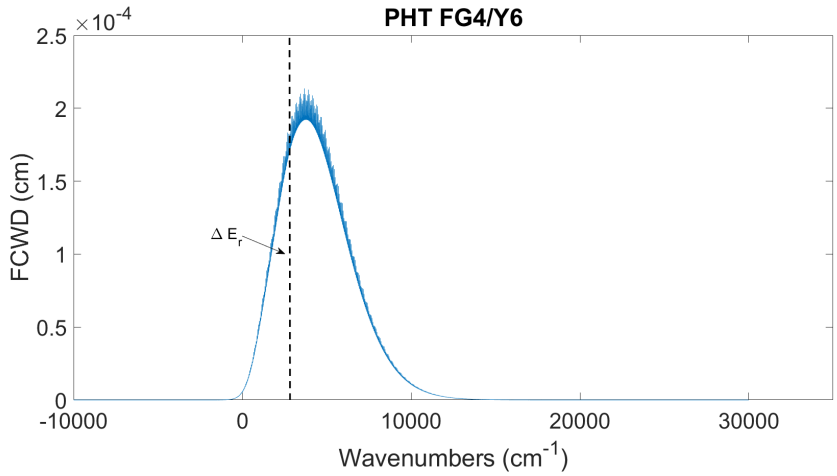

Fig. S11: FCWD for the photohole transfer process $\mathrm{Y6}^* + \mathrm{FG4} \rightarrow \mathrm{Y6}^- + \mathrm{FG4}^+$ obtained by convolution of the FCWDs for the $\mathrm{Y6}^* \rightarrow \mathrm{Y6}^-$ and $\mathrm{FG4} \rightarrow \mathrm{FG4}^+$ processes. The black dashed line indicates the energy of the reaction (ΔE_r) at which the FCWD is evaluated.

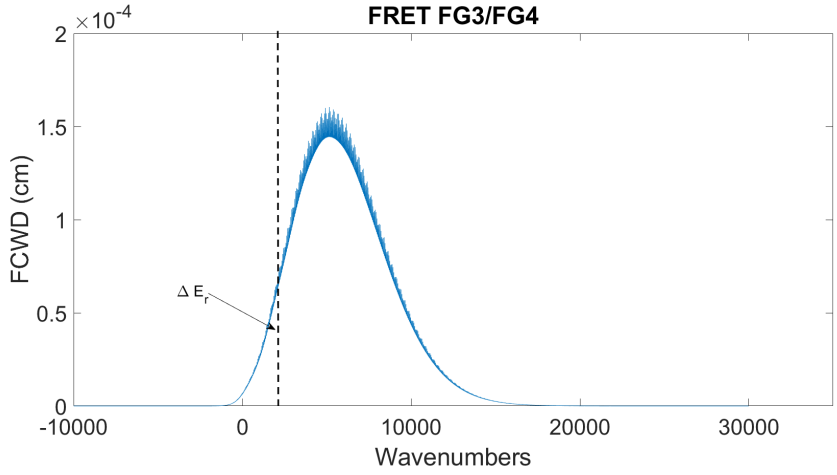

Fig. S12: FCWD for the Förster resonance energy transfer from $\mathrm{FG3}^*$ to FG4 obtained by convolution of the FCWDs for the $\mathrm{FG3}^* \rightarrow \mathrm{FG3}$ and $\mathrm{FG4} \rightarrow \mathrm{FG4}^*$ processes. The black dashed line indicates the energy of the reaction (ΔE_r) at which the FCWD is evaluated.

S5 Time dependent evolution of state populations with a reduced conformational sampling

In Fig. S13 we report the time-dependent evolution of the populations of the electronic states for FG3:Y6 and FG4:Y6, for an initial condition corresponding to a local excitation of the donor ($P_{D^*} = 1$), using transfer integral values computed on a reduced conformational space, i.e. sampling only from the last 20 ns of the MD simulations. Comparison with Fig. 3 in the main text shows that the time evolution remains qualitatively similar, ensuring that the sampling used to compute the rates used for the kinetic model is extensive enough to obtain a correct prediction of the average behaviour of the device.

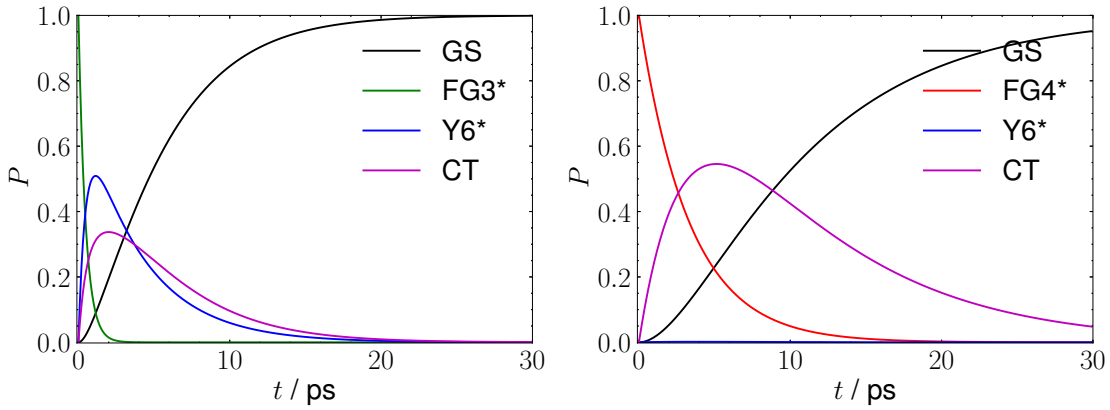

Fig. S13: Time dependent evolution of state populations for FG3:Y6 (left) and FG4:Y6 (right) using rates of . We consider an initial condition corresponding to a local excitation of the donor ($P_{D^*} = 1$). The labels GS, X* and CT refer, respectively, to the ground state, a local excitation on the molecule X, and the charge transfer state.

S6 Predicted SOC

In this section we report the spin-orbit coupling for the Intersystem Crossing between the first triplet excited state (T_1) and the ground state (S_0) and between the first singlet excited state (S_1) and T_1 for all the molecules under study.

Table S4: Spin-orbit coupling (SOC, cm^{-1}) for the Intersystem Crossing between the first triplet excited state (T_1) and the ground state (S_0) and between the first singlet excited state (S_1) and T_1. The former has been computed starting from the T_1 geometry, the latter starting from the S_1 geometry. All the couplings have been computed using the Orca software.[30]

Molecule	$SOC_{T_1 \rightarrow S_0}$	$SOC_{S_1 \rightarrow T_1}$ (cm^{-1})
FG3	0.11	0.01
FG4	0.25	0.01
Y6	0.11	0.06

References

[S1] F. G. Guijarro, R. Caballero, P. de la Cruz, R. Singhal, F. Langa and G. D. Sharma, *Solar RRL*, 2020, **4**, 2000460.

[S2] A. Landi and D. Padula, *J. Mater. Chem. A*, 2021, **9**, 24849–24856.

[S3] A. Landi, D. Padula and A. Peluso, *ACS Appl. Energy Mater.*, 2024, **7**, 707–714.

[S4] A. Troisi and G. Orlandi, *Chem. Phys. Lett.*, 2001, **344**, 509 – 518.

[S5] A. Landi and A. Troisi, *J. Phys. Chem. C*, 2018, **122**, 18336–18345.

[S6] T. Nematiaram, D. Padula, A. Landi and A. Troisi, *Adv. Funct. Mater.*, 2020, **30**, 2001906.

[S7] T. Yanai, D. P. Tew and N. C. Handy, *Chem. Phys. Lett.*, 2004, **393**, 51–57.

[S8] A. Muñoz-Losa, C. Curutchet, I. F. Galván and B. Mennucci, *J. Chem. Phys.*, 2008, **129**, 034104.

[S9] M. J. Frisch, G. W. Trucks, H. B. Schlegel, G. E. Scuseria, M. A. Robb, J. R. Cheeseman, G. Scalmani, V. Barone, G. A. Petersson, H. Nakatsuji, X. Li, M. Caricato, A. V. Marenich, J. Bloino, B. G. Janesko, R. Gomperts, B. Mennucci, H. P. Hratchian, J. V. Ortiz, A. F. Izmaylov, J. L. Sonnenberg, D. Williams-Young, F. Ding, F. Lipparini, F. Egidi, J. Goings, B. Peng, A. Petrone, T. Henderson, D. Ranasinghe, V. G. Zakrzewski, J. Gao, N. Rega, G. Zheng, W. Liang, M. Hada, M. Ehara, K. Toyota, R. Fukuda, J. Hasegawa, M. Ishida, T. Nakajima, Y. Honda, O. Kitao, H. Nakai, T. Vreven, K. Throssell, J. A. Montgomery, Jr., J. E. Peralta, F. Ogliaro, M. J. Bearpark, J. J. Heyd, E. N. Brothers, K. N. Kudin, V. N. Staroverov, T. A. Keith, R. Kobayashi, J. Normand, K. Raghavachari, A. P. Rendell, J. C. Burant, S. S. Iyengar, J. Tomasi, M. Cossi, J. M. Millam, M. Klene, C. Adamo, R. Cammi, J. W. Ochterski, R. L. Martin, K. Morokuma, O. Farkas, J. B. Foresman and D. J. Fox, *Gaussian 16 Revision C.01*, 2016, Gaussian Inc. Wallingford CT.

[S10] R. Kubo and Y. Toyozawa, *Prog. Theor. Phys.*, 1955, **13**, 160–182.

[S11] R. Borrelli and A. Peluso, *Phys. Chem. Chem. Phys.*, 2011, **13**, 4420–4426.

[S12] M. Lax, *J. Chem. Phys.*, 1952, **20**, 1752–1760.

[S13] F. Duschinsky, *Acta Physicochim. URSS*, 1937, **7**, 551–566.

[S14] F. G. Guijarro, P. Malhotra, G. Gupta, R. Caballero, P. de la Cruz, R. Singhal, G. D. Sharma and F. Langa, *J. Mater. Chem. C*, 2020, **8**, 4763–4770.

[S15] A. Capobianco, R. Borrelli, A. Landi, A. Velardo and A. Peluso, *J. Phys. Chem. A*, 2016, **120**, 5581–5589.

[S16] A. Velardo, R. Borrelli, A. Capobianco, A. Landi and A. Peluso, *J. Phys. Chem. C*, 2019, **123**, 14173–14179.

[S17] A. Landi, A. Landi, A. Velardo and A. Peluso, *ACS Appl. Energy Mater.*, 2022, **5**, 10815–10824.

[S18] G. D'Avino, L. Muccioli, C. Zannoni, D. Beljonne and Z. G. Soos, *J. Chem. Theory Comput.*, 2014, **10**, 4959–4971.

[S19] A. Landi, *J. Phys. Chem. C*, 2019, **123**, 18804–18812.

[S20] M. J. Abraham, T. Murtola, R. Schulz, S. Páll, J. C. Smith, B. Hess and E. Lindahl, *SoftwareX*, 2015, **1-2**, 19–25.

[S21] W. L. Jorgensen, D. S. Maxwell and J. Tirado-Rives, *J. Am. Chem. Soc.*, 1996, **118**, 11225–11236.

[S22] T. Darden, D. York and L. Pedersen, *J. Chem. Phys.*, 1993, **98**, 10089–10092.

[S23] B. Hess, H. Bekker, H. J. C. Berendsen and J. G. E. M. Fraaije, *J. Comput. Chem.*, 1997, **18**, 1463–1472.

[S24] H. J. C. Berendsen, J. P. M. Postma, W. F. van Gunsteren, A. DiNola and J. R. Haak, *J. Chem. Phys.*, 1984, **81**, 3684–3690.

[S25] M. Parrinello and A. Rahman, *J. Appl. Phys.*, 1981, **52**, 7182–7190.

[S26] S. Giannini, A. Carof and J. Blumberger, *J. Phys. Chem. Lett.*, 2018, **9**, 3116–3123.

[S27] R. Borrelli, A. Capobianco and A. Peluso, *MolFC: A program for Franck-Condon integrals calculation*, Package available online at `https://github.com/rborrelli/molfc`.

[S28] H. Sumi and T. Kakitani, *Chem. Phys. Lett.*, 1996, **252**, 85–93.

[S29] T. Renger and R. A. Marcus, *J. Phys. Chem. A*, 2003, **107**, 8404–8419.

[S30] F. Neese, *Wiley Interdiscip. Rev. Comput. Mol. Sci.*, 2012, **2**, 73–78.